Journal of Guidance, Control, and Dynamics, Vol. 44, No. 4, 2021, pp. 889–897. doi: https://doi.org/10.2514/1.G005624

Time-Optimal Formation Establishment Around a Slowly Rotating Asteroid

Wei Wang*
School of Aerospace Engineering, Tsinghua University, 100084 Beijing, People's Republic of China
Giovanni Mengali†, Alessandro A. Quarta‡
Department of Civil and Industrial Engineering, University of Pisa, I-56122 Pisa, Italy
and
Hexi Baoyin§
School of Aerospace Engineering, Tsinghua University, 100084 Beijing, People's Republic of China

Introduction

Asteroids' exploration has drawn a growing interest since the early 1990s, when NASA, ESA, and JAXA successively proposed their task plans [1,2] in which asteroids were considered a primary goal for new millennium spacecraft missions. Indeed, an in-depth analysis of asteroid samples may substantially improve the human knowledge of the Solar System evolution [3], while the exploration of near-Earth objects is meaningful for planetary defense purposes [4]. In this regard, following the tracks of the first successful sample return prober Hayabusa [5], the Japanese space prober Hayabusa-2 has successfully fired an impactor into its target asteroid 162173 Ryugu to create an artificial crater [6]. The splashing rock ash has allowed the spacecraft to collect asteroid samples placed beneath its surface [7].

Some advanced mission concepts, such as NASA Autonomous Nano-Technology Swarm (ANTS), require a collaborative framework with hierarchical (multilevel, dense heterarchy) organization and high autonomy, as well as redundant components with a certain degree of flexibility [8]. Other mission scenarios, consisting in the use of a spacecraft formation system for asteroid deflection [9–12], require an advanced (onboard) autonomous formation flying control system. In fact, from an operational standpoint, it is preferable to deploy a formation along suitable hovering [13] or periodic orbits [14,15] around the target asteroid in order to initiate the asteroid gravity database and to chart a local geomorphologic map. When multiple spacecraft operate in close proximity, a (virtual) synthetic aperture radar can be ideally assembled [16] to improve the resolution of stereoscopic images, with a substantial reduction of the overall mission cost. In this scenario, the consensus concept guarantees a functional module distribution among the spacecraft in the formation [17,18], in such a way as to eliminate the inherent single point of failure of the on-board system [19,20].

So far, most of the existing literature [21,22] has been dedicated to study the spacecraft relative motion in the presence of J_2 term, i.e., the most relevant perturbation for spacecraft formations in low-Earth orbits [23,24], whereas the problem of spacecraft relative motion around an asteroid has been rarely addressed [25,26]. In fact, the complex weak nature of the asteroid gravity enables only a few types of stable orbits to be obtained [27], e.g. the quasi-frozen orbits [28]. For this reason the relative spacecraft dynamics around an asteroid is much more complex than that involving the J_2 effect only and, in this case, the differential gravity among the formation spacecraft may induce a rapid growth of their relative distance. Especially for those long-term maintenance missions, an active control system is usually necessary to prevent the spacecraft formation from colliding with or escaping from the asteroid, and hence, a considerable fuel consumption is usually required.

The aim of this Note is to deal with the problem of time-optimal formation establishment around a slowly rotating (uniform) asteroid, whose gravity is approximated as a second-degree and second-order gravitational field (SDSOGF). Similar to the methodology used for identifying the classical J_2-invariant relative orbits, two necessary conditions are analytically derived to guarantee bounded relative motion in a SDSOGF. In particular, it is shown that when the non-spherical harmonic coefficients of the asteroid gravity are first-order small, the resulting necessary conditions are consistent with the recent literature results [29]. In this sense, since general boundedness conditions (not necessarily related to the quasi-frozen case) are provided by the proposed approach, this Note extends the results of Ref. [29]. Moreover, the discussed mathematical model introduces a method to reduce the relative (secular) drift induced by the mean eccentricity of the chief spacecraft. Based on the (analytically) obtained constraints, the problem of time-optimal formation establishment is then emphasized via an indirect approach, in which the initial (unknown) costate vector is calculated with a scaling technique to alleviate its sensitivity to the initial guess problem.

General Conditions for Bounded Relative Motion

Consider a spacecraft orbiting around an asteroid, which is approximated by an ellipsoid of uniform density. Assume that the asteroid rotates about its maximum axis of inertia at a constant rate $n_T \ll n$, where n is the mean motion of the spacecraft orbit. According to Refs. [28,30], the averaged gravitational (perturbing) potential $\bar{\mathcal{R}}$ in a SDSOGF can be approximated as

$$\bar{\mathcal{R}} \simeq \frac{\mu R_0^2}{2\,\bar{a}^3\,(1-\bar{e}^2)^{\frac{3}{2}}} \left[C_{20}\left(\frac{3}{2}\sin^2\bar{i}-1\right)+3\,C_{22}\,\sin^2\bar{i}\,\cos\left(2\,\bar{\Omega}_R\right)\right] \tag{1}$$

*Research Assistant, wei_wang@mail.tsinghua.edu.cn.
†Professor, g.mengali@ing.unipi.it. Senior Member AIAA.
‡Professor, a.quarta@ing.unipi.it. Associate Fellow AIAA
§Professor, baoyin@tsinghua.edu.cn. Senior Member AIAA (**corresponding author**).

where μ is the asteroid gravitational parameter, R_0 is the normalizing distance, defined as the radius of the sphere of equal volume, while C_{20} and C_{22} are the harmonic (Stokes) coefficients. In Eq. (1), the overbar $(\bar{\cdot})$ refers to the mean value, and $\bar{a}, \bar{e}$, and $\bar{i}$ are, respectively, the semimajor axis, eccentricity, and inclination of the spacecraft mean orbit, while $\bar{\Omega}_R \triangleq \bar{\Omega} - n_T\, t$, where $\bar{\Omega}$ is the ascending node longitude of the spacecraft mean orbit.

Substituting Eq. (1) into the Lagrange planetary equations [31], the time-variation of the spacecraft mean orbital elements are

$$\frac{\mathrm{d}\bar{a}}{\mathrm{d}t} = 0 \tag{2}$$

$$\frac{\mathrm{d}\bar{e}}{\mathrm{d}t} = 0 \tag{3}$$

$$\frac{\mathrm{d}\bar{i}}{\mathrm{d}t} = \frac{3\,\bar{n}\,C_{22}}{(\bar{p}/R_0)^2}\,\sin\bar{i}\,\sin 2\,\bar{\Omega}_R \tag{4}$$

$$\frac{\mathrm{d}\bar{\Omega}_R}{\mathrm{d}t} = \frac{3\,\bar{n}\,\cos\bar{i}}{2\,(\bar{p}/R_0)^2}\,\left(C_{20} + 2\,C_{22}\,\cos 2\,\bar{\Omega}_R\right) - n_T \tag{5}$$

$$\frac{\mathrm{d}\bar{\omega}}{\mathrm{d}t} = -\frac{3\,\bar{n}}{8\,(\bar{p}/R_0)^2}\,\left(3\,C_{20} + 5\,C_{20}\,\cos 2\,\bar{i} - 2\,C_{22}\,\cos 2\,\bar{\Omega}_R + 10\,C_{22}\,\cos 2\,\bar{i}\,\cos 2\,\bar{\Omega}_R\right) \tag{6}$$

$$\frac{\mathrm{d}\bar{M}}{\mathrm{d}t} = \bar{n} - \frac{3\,\bar{n}\,\sqrt{1-\bar{e}^2}}{8\,(\bar{p}/R_0)^2}\,\left(C_{20} + 3\,C_{20}\,\cos 2\,\bar{i} - 6\,C_{22}\,\cos 2\,\bar{\Omega}_R + 6\,C_{22}\,\cos 2\,\bar{i}\,\cos 2\,\bar{\Omega}_R\right) \tag{7}$$

where $\bar{p} = \bar{a}\,\left(1-\bar{e}^2\right)$ is the semilatus rectum, $\bar{n} = \sqrt{\mu/\bar{a}^3}$ is the mean motion, $\bar{\omega}$ is the argument of pericenter, and $\bar{M}$ is the spacecraft mean anomaly. In particular, Eqs. (2)–(7) state that $\bar{a}$ and $\bar{e}$ are constants of motion, whereas the remaining elements $\bar{i}$, $\bar{\Omega}_R$, $\bar{\omega}$ and $\bar{M}$, which are a function of $\left\{\bar{a}, \bar{e}, \bar{i}, \bar{\Omega}_R\right\}$, have long-period and/or secular variations.

Consider now the relative motion of two spacecraft, referred to as chief and deputy, which fly in a SDSOGF around a target asteroid. For convenience, denote $\mathcal{F}_{\bar{x}} \triangleq \mathrm{d}\bar{x}/\mathrm{d}t$, with $x = \{i, \Omega_R, \omega, M\}$, so that the generic $\mathcal{F}_{\bar{x}}$ is a function of $\bar{x}$ through Eqs. (4)–(7). Taking the first-order variations of Eqs. (4)–(7) yields

$$\delta\dot{\bar{i}} = \frac{\partial\mathcal{F}_{\bar{i}}}{\partial\bar{a}}\,\delta\bar{a} + \frac{\partial\mathcal{F}_{\bar{i}}}{\partial\bar{e}}\,\delta\bar{e} + \frac{\partial\mathcal{F}_{\bar{i}}}{\partial\bar{i}}\,\delta\bar{i} + \frac{\partial\mathcal{F}_{\bar{i}}}{\partial\bar{\Omega}_R}\,\delta\bar{\Omega}_R \tag{8}$$

$$\delta\dot{\bar{\Omega}}_R = \frac{\partial\mathcal{F}_{\bar{\Omega}_R}}{\partial\bar{a}}\,\delta\bar{a} + \frac{\partial\mathcal{F}_{\bar{\Omega}_R}}{\partial\bar{e}}\,\delta\bar{e} + \frac{\partial\mathcal{F}_{\bar{\Omega}_R}}{\partial\bar{i}}\,\delta\bar{i} + \frac{\partial\mathcal{F}_{\bar{\Omega}_R}}{\partial\bar{\Omega}_R}\,\delta\bar{\Omega}_R \tag{9}$$

$$\delta\dot{\bar{\omega}} = \frac{\partial\mathcal{F}_{\bar{\omega}}}{\partial\bar{a}}\,\delta\bar{a} + \frac{\partial\mathcal{F}_{\bar{\omega}}}{\partial\bar{e}}\,\delta\bar{e} + \frac{\partial\mathcal{F}_{\bar{\omega}}}{\partial\bar{i}}\,\delta\bar{i} + \frac{\partial\mathcal{F}_{\bar{\omega}}}{\partial\bar{\Omega}_R}\,\delta\bar{\Omega}_R \tag{10}$$

$$\delta\dot{\bar{M}} = \frac{\partial\mathcal{F}_{\bar{M}}}{\partial\bar{a}}\,\delta\bar{a} + \frac{\partial\mathcal{F}_{\bar{M}}}{\partial\bar{e}}\,\delta\bar{e} + \frac{\partial\mathcal{F}_{\bar{M}}}{\partial\bar{i}}\,\delta\bar{i} + \frac{\partial\mathcal{F}_{\bar{M}}}{\partial\bar{\Omega}_R}\,\delta\bar{\Omega}_R \tag{11}$$

where the partial derivatives are reported in the Appendix for completeness. To prevent the chief and deputy from drifting apart, it is straightforward to impose the following constraints

$$\delta\dot{\bar{i}} = 0 \quad \cap \quad \delta\dot{\bar{\Omega}}_R = 0 \quad \cap \quad \delta\dot{\bar{\omega}} = 0 \quad \cap \quad \delta\dot{\bar{M}} = 0 \tag{12}$$

In the general case when the determinant of the coefficients matrix of the linear system represented by Eqs. (8)–(11) is different from zero, Eq. (12) only allows the trivial solution $\delta\,\bar{a} = \delta\,\bar{e} = \delta\,\bar{i} = \delta\,\bar{\Omega}_R = 0$. Thus, once the chief orbit is prescribed, the only degrees of freedom in the formation structure are $\delta\bar{\omega}$ and $\delta\bar{M}$. As a result, only a few planar formations are feasible, which may be incompatible with practical mission requirements.

Alternatively, motivated by the approach for identifying the J_2-invariant relative motion [21], the following constraints may be enforced

$$\delta\dot{\bar{i}} = 0 \quad \cap \quad \delta\dot{\bar{\Omega}}_R = 0 \quad \cap \quad \delta\dot{\bar{\omega}} + \kappa\,\delta\dot{\bar{M}} = 0 \tag{13}$$

where κ is a sort of correcting (dimensionless) parameter, given by [32]

$$\kappa \triangleq \frac{1-\bar{e}}{(1-\bar{e}-2\,\bar{e}^2)\,\sqrt{1-\bar{e}^2}} \tag{14}$$

which is introduced to (further) reduce the along-track relative drift caused by the eccentricity of the chief orbit. Substituting Eqs. (8)–(11) into Eq. (13), the general boundedness conditions for spacecraft relative motion in a SDSOGF are obtained as

$$\delta\bar{a} = \frac{\det\mathbb{F}_{\bar{a}}}{\det\mathbb{F}}\,\delta\bar{e}, \quad \delta\bar{i} = -\frac{\det\mathbb{F}_{\bar{i}}}{\det\mathbb{F}}\,\delta\bar{e}, \quad \delta\bar{\Omega}_R = -\frac{\det\mathbb{F}_{\bar{\Omega}_R}}{\det\mathbb{F}}\,\delta\bar{e} \tag{15}$$

where the matrices $\{\mathbb{F}, \mathbb{F}_{\bar{a}}, \mathbb{F}_{\bar{i}}, \mathbb{F}_{\bar{\Omega}_R}\}$ are defined as

$$\mathbb{F} = \begin{bmatrix} \dfrac{\partial \mathcal{F}_{\bar{i}}}{\partial \bar{a}} & \dfrac{\partial \mathcal{F}_{\bar{i}}}{\partial \bar{i}} & \dfrac{\partial \mathcal{F}_{\bar{i}}}{\partial \bar{\Omega}_R} \\ \dfrac{\partial \mathcal{F}_{\bar{\Omega}_R}}{\partial \bar{a}} & \dfrac{\partial \mathcal{F}_{\bar{\Omega}_R}}{\partial \bar{i}} & \dfrac{\partial \mathcal{F}_{\bar{\Omega}_R}}{\partial \bar{\Omega}_R} \\ \dfrac{\partial \mathcal{F}_{\bar{\omega}}}{\partial \bar{a}} + \kappa\, \dfrac{\partial \mathcal{F}_{\bar{M}}}{\partial \bar{a}} & \dfrac{\partial \mathcal{F}_{\bar{\omega}}}{\partial \bar{i}} + \kappa\, \dfrac{\partial \mathcal{F}_{\bar{M}}}{\partial \bar{i}} & \dfrac{\partial \mathcal{F}_{\bar{\omega}}}{\partial \bar{\Omega}_R} + \kappa\, \dfrac{\partial \mathcal{F}_{\bar{M}}}{\partial \bar{\Omega}_R} \end{bmatrix} \tag{16}$$

$$\mathbb{F}_{\bar{a}} = \begin{bmatrix} \dfrac{\partial \mathcal{F}_{\bar{i}}}{\partial \bar{e}} & \dfrac{\partial \mathcal{F}_{\bar{i}}}{\partial \bar{i}} & \dfrac{\partial \mathcal{F}_{\bar{i}}}{\partial \bar{\Omega}_R} \\ \dfrac{\partial \mathcal{F}_{\bar{\Omega}_R}}{\partial \bar{e}} & \dfrac{\partial \mathcal{F}_{\bar{\Omega}_R}}{\partial \bar{i}} & \dfrac{\partial \mathcal{F}_{\bar{\Omega}_R}}{\partial \bar{\Omega}_R} \\ \dfrac{\partial \mathcal{F}_{\bar{\omega}}}{\partial \bar{e}} + \kappa\, \dfrac{\partial \mathcal{F}_{\bar{M}}}{\partial \bar{e}} & \dfrac{\partial \mathcal{F}_{\bar{\omega}}}{\partial \bar{i}} + \kappa\, \dfrac{\partial \mathcal{F}_{\bar{M}}}{\partial \bar{i}} & \dfrac{\partial \mathcal{F}_{\bar{\omega}}}{\partial \bar{\Omega}_R} + \kappa\, \dfrac{\partial \mathcal{F}_{\bar{M}}}{\partial \bar{\Omega}_R} \end{bmatrix} \tag{17}$$

$$\mathbb{F}_{\bar{i}} = \begin{bmatrix} \dfrac{\partial \mathcal{F}_{\bar{i}}}{\partial \bar{a}} & \dfrac{\partial \mathcal{F}_{\bar{i}}}{\partial \bar{e}} & \dfrac{\partial \mathcal{F}_{\bar{i}}}{\partial \bar{\Omega}_R} \\ \dfrac{\partial \mathcal{F}_{\bar{\Omega}_R}}{\partial \bar{a}} & \dfrac{\partial \mathcal{F}_{\bar{\Omega}_R}}{\partial \bar{e}} & \dfrac{\partial \mathcal{F}_{\bar{\Omega}_R}}{\partial \bar{\Omega}_R} \\ \dfrac{\partial \mathcal{F}_{\bar{\omega}}}{\partial \bar{a}} + \kappa\, \dfrac{\partial \mathcal{F}_{\bar{M}}}{\partial \bar{a}} & \dfrac{\partial \mathcal{F}_{\bar{\omega}}}{\partial \bar{e}} + \kappa\, \dfrac{\partial \mathcal{F}_{\bar{M}}}{\partial \bar{e}} & \dfrac{\partial \mathcal{F}_{\bar{\omega}}}{\partial \bar{\Omega}_R} + \kappa\, \dfrac{\partial \mathcal{F}_{\bar{M}}}{\partial \bar{\Omega}_R} \end{bmatrix} \tag{18}$$

$$\mathbb{F}_{\bar{\Omega}_R} = \begin{bmatrix} \dfrac{\partial \mathcal{F}_{\bar{i}}}{\partial \bar{a}} & \dfrac{\partial \mathcal{F}_{\bar{i}}}{\partial \bar{i}} & \dfrac{\partial \mathcal{F}_{\bar{i}}}{\partial \bar{e}} \\ \dfrac{\partial \mathcal{F}_{\bar{\Omega}_R}}{\partial \bar{a}} & \dfrac{\partial \mathcal{F}_{\bar{\Omega}_R}}{\partial \bar{i}} & \dfrac{\partial \mathcal{F}_{\bar{\Omega}_R}}{\partial \bar{e}} \\ \dfrac{\partial \mathcal{F}_{\bar{\omega}}}{\partial \bar{a}} + \kappa\, \dfrac{\partial \mathcal{F}_{\bar{M}}}{\partial \bar{a}} & \dfrac{\partial \mathcal{F}_{\bar{\omega}}}{\partial \bar{i}} + \kappa\, \dfrac{\partial \mathcal{F}_{\bar{M}}}{\partial \bar{i}} & \dfrac{\partial \mathcal{F}_{\bar{\omega}}}{\partial \bar{e}} + \kappa\, \dfrac{\partial \mathcal{F}_{\bar{M}}}{\partial \bar{e}} \end{bmatrix} \tag{19}$$

Using the constraints given by Eq. (15), the secular growth of spacecraft relative distance can be suitably mitigated. Moreover, since the motion near a certain special orbits, e.g. the frozen [33] and quasi-frozen orbits [28, 30], is linearly stable, these typical trajectories are usually suggested for spacecraft formation flying [29, 33, 34]. Therefore, if some flexibility is allowed in specifying the chief nominal orbit, such a degree of freedom may be used to initialize a passive relative motion that is adequate for formation flying around the target asteroid. In what follows, the boundedness conditions for relative motion around a quasi-frozen orbit will be recovered.

According to Ref. [28], a perfect frozen orbit does not exist in a SDSOGF, because the argument of periapsis $\bar{\omega}$ always exhibits a nonzero variation; see Eq. (6). However, some quasi-frozen orbits, whose value of $\bar{i}$ and $\bar{\Omega}_R$ are both stationary, can still be obtained. For example, taking into account Eqs. (4)–(5), when $n_T < 3\,\bar{n}\,R_0^2\,(2\,C_{22} - C_{20})\,/\,(2\,\bar{p}^2)$, the conditions $\mathrm{d}\bar{i}/\mathrm{d}t = \mathrm{d}\bar{\Omega}_R/\mathrm{d}t = 0$ give [29, 30]

$$\bar{\Omega}_R = \frac{\pi}{2}, \quad \bar{i} = \arccos\left[\frac{2\,n_T\,\bar{p}^2}{3\,\bar{n}\,R_0^2\,(C_{20} - 2\,C_{22})}\right] \tag{20}$$

The quasi-frozen orbits satisfying Eq. (20) are linearly stable in the $(\bar{i}, \bar{\Omega}_R)$ phase space, despite the argument of periapsis $\bar{\omega}$ has a constant secular rate; see Eq. (6). Note that, apart from the quasi-frozen orbits represented by Eq. (20), there also exist other families of stable orbits such as the prograde equatorial orbits [28]. Moreover, it is possible to get orbits with constant (on average) eccentricity and argument of pericentre by removing the constraint of frozen attitude of the orbital plane with respect to the asteroid [35, 36].

Consider now the formation flying of two spacecraft, where the chief moves along a nominal quasi-frozen orbit, while the deputy flies nearby. When evaluated with the parameters given by Eq. (20), Eqs. (.1)–(.3) imply that $\partial \mathcal{F}_{\bar{i}}/\partial \bar{a} = \partial \mathcal{F}_{\bar{i}}/\partial \bar{e} = \partial \mathcal{F}_{\bar{i}}/\partial \bar{\Omega}_R = 0$. In that case, Eq. (19) provides $\det \mathbb{F}_{\bar{\Omega}_R} \equiv 0$, and thus Eq. (15) gives $\delta \bar{\Omega}_R = 0$. Accordingly, the degenerated form of boundedness condition given by Eq. (15) can be rewritten as

$$\delta\bar{a} = \frac{\dfrac{\partial \mathcal{F}_{\bar{\Omega}_R}}{\partial \bar{i}}\left(\dfrac{\partial \mathcal{F}_{\bar{\omega}}}{\partial \bar{e}} + \kappa\,\dfrac{\partial \mathcal{F}_{\bar{M}}}{\partial \bar{e}}\right) - \dfrac{\partial \mathcal{F}_{\bar{\Omega}_R}}{\partial \bar{e}}\left(\dfrac{\partial \mathcal{F}_{\bar{\omega}}}{\partial \bar{i}} + \kappa\,\dfrac{\partial \mathcal{F}_{\bar{M}}}{\partial \bar{i}}\right)}{\dfrac{\partial \mathcal{F}_{\bar{\Omega}_R}}{\partial \bar{a}}\left(\dfrac{\partial \mathcal{F}_{\bar{\omega}}}{\partial \bar{i}} + \kappa\,\dfrac{\partial \mathcal{F}_{\bar{M}}}{\partial \bar{i}}\right) - \dfrac{\partial \mathcal{F}_{\bar{\Omega}_R}}{\partial \bar{i}}\left(\dfrac{\partial \mathcal{F}_{\bar{\omega}}}{\partial \bar{a}} + \kappa\,\dfrac{\partial \mathcal{F}_{\bar{M}}}{\partial \bar{a}}\right)}\,\delta\bar{e} \tag{21}$$

$$\delta\bar{i} = \frac{\dfrac{\partial \mathcal{F}_{\bar{\Omega}_R}}{\partial \bar{e}}\left(\dfrac{\partial \mathcal{F}_{\bar{\omega}}}{\partial \bar{a}} + \kappa\,\dfrac{\partial \mathcal{F}_{\bar{M}}}{\partial \bar{a}}\right) - \dfrac{\partial \mathcal{F}_{\bar{\Omega}_R}}{\partial \bar{a}}\left(\dfrac{\partial \mathcal{F}_{\bar{\omega}}}{\partial \bar{e}} + \kappa\,\dfrac{\partial \mathcal{F}_{\bar{M}}}{\partial \bar{e}}\right)}{\dfrac{\partial \mathcal{F}_{\bar{\Omega}_R}}{\partial \bar{a}}\left(\dfrac{\partial \mathcal{F}_{\bar{\omega}}}{\partial \bar{i}} + \kappa\,\dfrac{\partial \mathcal{F}_{\bar{M}}}{\partial \bar{i}}\right) - \dfrac{\partial \mathcal{F}_{\bar{\Omega}_R}}{\partial \bar{i}}\left(\dfrac{\partial \mathcal{F}_{\bar{\omega}}}{\partial \bar{a}} + \kappa\,\dfrac{\partial \mathcal{F}_{\bar{M}}}{\partial \bar{a}}\right)}\,\delta\bar{e} \tag{22}$$

In particular, if the eccentricity of the chief orbit is sufficiently small, it is reasonable to neglect the terms including $\bar{e}^2$ in Eqs. (.1)–(.16), when substituting them into Eqs. (21)–(22). The result is

$$\delta\bar{a} = \frac{\left[7\,C_{20}\,\left(1 + 5\,\cos^2\bar{i}\right) - 3\,C_{22}\,\left(7 + 33\,\cos^2\bar{i}\right)\right]\,\bar{a}\,\bar{e}}{2\,\left(\bar{a}/R_0\right)^2 + 7\,C_{20}\,\left(1 + 4\,\cos^2\bar{i}\right) - 14\,C_{22}\,\left(3 + 4\,\cos^2\bar{i}\right)}\,\delta\bar{e} \tag{23}$$

$$\delta\bar{i} = \frac{\left[16\,\left(\bar{a}/R_0\right)^2 + 7\,C_{20}\,\left(1 - 3\,\cos^2\bar{i}\right) - 42\,C_{22}\,\left(1 - \cos^2\bar{i}\right)\right]\,\bar{e}}{\left[4\,\left(\bar{a}/R_0\right)^2 + 14\,C_{20}\,\left(1 + 4\,\cos^2\bar{i}\right) - 28\,C_{22}\,\left(3 + 4\,\cos^2\bar{i}\right)\right]\,\tan\bar{i}}\,\delta\bar{e} \tag{24}$$

Note that, when the harmonic coefficients $\{C_{20}, C_{22}\}$ are first-order small, Eqs. (23)–(24) coincide with the results discussed in Ref. [29], which are obtained with a perturbed Hamiltonian via Delaunay elements for quasi-frozen orbits. Moreover, if the nominal orbit is nearly circular, the conditions given by Eqs. (23)–(24) are consistent with the results of Ref. [29]. Finally, for the case $C_{22} = 0$ (recall that $C_{20} = -J_2$), Eqs. (23)–(24) reduce to the well known J_2-invariant conditions [21, 32].

Having analyzed the bounded relative motion conditions necessary for spacecraft formation flying in a SDSOGF, a natural question that now arises is how to establish an optimal (loose) formation with a given performance index. The next section will analyze such a problem in terms of minimum time necessary for constituting a given formation structure.

Time-Optimal Formation Establishment

Consider a spacecraft of mass m, equipped with a low-continuous-thrust propulsion system of constant specific impulse $I_{\rm sp}$ and a thrust magnitude variable in the range $T \in [0, T_{\max}]$. To avoid any singularity, the spacecraft trajectory is studied in terms of modified equinoctial orbital elements (MEOEs) $\boldsymbol{\text{æ}} \triangleq \{p, f, g, h, k, L\}$ [37, 38], where

$$p = a\,\left(1 - e^2\right) \tag{25}$$
$$f = e\,\cos\left(\Omega_R + \omega\right) \tag{26}$$
$$g = e\,\sin\left(\Omega_R + \omega\right) \tag{27}$$
$$h = \cos\Omega_R\,\tan\frac{i}{2} \tag{28}$$
$$k = \sin\Omega_R\,\tan\frac{i}{2} \tag{29}$$
$$L = \Omega_R + \omega + \nu \tag{30}$$

in which ν is the true anomaly. Since the boundedness conditions are defined in the mean-element space, it is necessary to formulate the optimal problem in terms of mean MEOEs. To this end, let $\bar{\boldsymbol{\text{æ}}} = \boldsymbol{\xi}\left(\boldsymbol{\text{æ}}\right)$ denote the analytical transformation from osculating to mean MEOEs. Paralleling the procedure discussed in Ref. [39], the spacecraft dynamics in a SDSOGF can be described as

$$\dot{\bar{\boldsymbol{\text{æ}}}} = \mathbb{A}\left(\bar{\boldsymbol{\text{æ}}}\right) + \frac{T_{\max}\,\tau}{m}\,\frac{\partial\boldsymbol{\xi}}{\partial\boldsymbol{\text{æ}}}\,\mathbb{B}\left(\boldsymbol{\text{æ}}\right)\,\hat{\boldsymbol{\alpha}} \tag{31}$$

$$\dot{m} = -\frac{T_{\max}\,\tau}{I_{\rm sp}\,g_0} \tag{32}$$

with

$$\mathbb{A}\left(\bar{\boldsymbol{\text{æ}}}\right) = \left[0,\ \mathbb{A}_2,\ \mathbb{A}_3,\ \mathbb{A}_4,\ \mathbb{A}_5,\ \mathbb{A}_6\right]^{\rm T} \tag{33}$$

while the control influence matrix $\mathbb{B}$ is defined as

$$\mathbb{B}\left(\boldsymbol{\text{æ}}\right) = \begin{bmatrix} 0 & \mathbb{B}_{12} & 0 \\ \mathbb{B}_{21} & \mathbb{B}_{22} & \mathbb{B}_{23} \\ \mathbb{B}_{31} & \mathbb{B}_{32} & \mathbb{B}_{33} \\ 0 & 0 & \mathbb{B}_{43} \\ 0 & 0 & \mathbb{B}_{53} \\ 0 & 0 & \mathbb{B}_{63} \end{bmatrix} \tag{34}$$

where g_0 is the standard gravity, $\tau \triangleq T/T_{\max} \in [0,1]$ is a dimensionless parameter that models the engine throttle level, and $\hat{\boldsymbol{\alpha}}$ is the thrust unit vector. The detailed expressions of entries of $\mathbb{A}(\bar{\boldsymbol{æ}})$ and $\mathbb{B}(\boldsymbol{æ})$, which can be analytically evaluated using the Lagrange planetary equations [31], are rather involved and are not reported here for the sake of brevity.

According to Ref. [39], the influence of the propulsive acceleration on mean elements can be approximated as that on the corresponding osculating elements for the low-thrust case, because the induced error in the relative dynamics is negligible [39]. Therefore, it is reasonable to assume $\partial\boldsymbol{\xi}/\partial\boldsymbol{æ} \simeq \mathbb{I}_6$ and $\mathbb{B}(\bar{\boldsymbol{æ}}) \simeq \mathbb{B}(\boldsymbol{æ})$, where $\mathbb{I}_6 \in \mathbb{R}^{6\times 6}$ is an identity matrix. Accordingly, Eq. (31) can be further simplified as

$$\dot{\bar{\boldsymbol{æ}}} = \mathbb{A}(\bar{\boldsymbol{æ}}) + \frac{T_{\max}\,\tau}{m}\,\mathbb{B}(\bar{\boldsymbol{æ}})\,\hat{\boldsymbol{\alpha}} \tag{35}$$

where $\mathbb{B}(\bar{\boldsymbol{æ}})$ is obtained from Eq. (34) by simply replacing the generic osculating MEOEs with the corresponding mean MEOEs.

Assume the chief and deputy are both initially deployed along a nominal orbit at time $t_0 = 0$, with $\bar{\boldsymbol{æ}}_C(t_0) = \bar{\boldsymbol{æ}}_D(t_0) = \bar{\boldsymbol{æ}}_0$. The chief is subjected to the natural force only, whereas the deputy with active control is driven toward its design orbit so as to constitute the formation structure. According to Eq. (15) (or to Eqs. (21)–(22)) for the general (or the frozen-type) case, a given value of $\delta\bar{e}_f$ determines the required constraints on $\delta\bar{a}_f$, $\delta\bar{i}_f$, and $\delta\bar{\Omega}_{R_f}$. In terms of mean MEOEs, the final states of the deputy satisfying the bounded relative motion conditions are

$$\bar{p}(t_f) = \bar{p}_f, \quad \bar{f}^2(t_f) + \bar{g}^2(t_f) = \bar{f}_f^2 + \bar{g}_f^2, \quad \bar{h}(t_f) = \bar{h}_f, \quad \bar{k}(t_f) = \bar{k}_f \tag{36}$$

Note that the deputy's final true longitude $\bar{L}_f$ and argument of pericenter $\bar{\omega}_f$ are usually related to the specific mission requirement. In the following analysis, a loose formation is assumed so that a strict formation geometry is not required, and $\bar{L}_f$ and $\bar{\omega}_f$ are both left free.

The problem of spacecraft formation establishment is formulated within an optimal framework, by looking for the optimal control law $\tau = \tau^\star(t)$ and $\hat{\boldsymbol{\alpha}} = \hat{\boldsymbol{\alpha}}^\star(t)$ that minimizes the time interval $\Delta t = t_f - t_0 \equiv t_f$ with the previously discussed boundedness conditions. The performance index to be minimized is therefore

$$J \triangleq \lambda_0\, t_f \tag{37}$$

where the scaling factor $\lambda_0 \in \mathbb{R}^+$ is introduced to restrict the costate vector to lie on a unit hypersphere, useful for relieving its inherent sensitivity to the initial guess [40]. From Eqs. (32) and (35), the Hamiltonian function $\mathcal{H}$ can be written as

$$\mathcal{H} = \mathbb{A}(\bar{\boldsymbol{æ}})\cdot\boldsymbol{\lambda}_{\bar{æ}} + \frac{T_{\max}\,\tau}{m}\,\mathbb{B}(\bar{\boldsymbol{æ}})\,\hat{\boldsymbol{\alpha}}\cdot\boldsymbol{\lambda}_{\bar{æ}} - \frac{\lambda_m\,T_{\max}\,\tau}{I_{\rm sp}\,g_0} + \lambda_0 \tag{38}$$

where λ_m is the mass costate, and $\boldsymbol{\lambda}_{\bar{æ}}$ is the vector adjoint to $\bar{\boldsymbol{æ}}$, defined as

$$\boldsymbol{\lambda}_{\bar{æ}} \triangleq \left[\lambda_{\bar{p}}, \lambda_{\bar{f}}, \lambda_{\bar{g}}, \lambda_{\bar{h}}, \lambda_{\bar{k}}, \lambda_{\bar{L}}\right]^{\rm T} \tag{39}$$

whose time derivatives are given by the Euler-Lagrange equations

$$\dot{\boldsymbol{\lambda}}_{\bar{æ}} = -\frac{\partial\mathcal{H}}{\partial\bar{\boldsymbol{æ}}} = -\frac{\partial\left[\mathbb{A}(\bar{\boldsymbol{æ}})\cdot\boldsymbol{\lambda}_{\bar{æ}}\right]}{\partial\bar{\boldsymbol{æ}}} - \frac{T_{\max}\,\tau}{m}\,\frac{\partial\left(\boldsymbol{\eta}_{\bar{æ}}\cdot\hat{\boldsymbol{\alpha}}\right)}{\partial\bar{\boldsymbol{æ}}} \tag{40}$$

$$\dot{\lambda}_m = -\frac{\partial\mathcal{H}}{\partial m} = \frac{T_{\max}\,\tau}{m^2}\,\boldsymbol{\eta}_{\bar{æ}}\cdot\hat{\boldsymbol{\alpha}} \tag{41}$$

where

$$\boldsymbol{\eta}_{\bar{æ}} \triangleq \mathbb{B}^{\rm T}(\bar{\boldsymbol{æ}})\,\boldsymbol{\lambda}_{\bar{æ}} = \begin{bmatrix} \lambda_{\bar{f}}\,\mathbb{B}_{21} + \lambda_{\bar{g}}\,\mathbb{B}_{31} \\ \lambda_{\bar{p}}\,\mathbb{B}_{12} + \lambda_{\bar{f}}\,\mathbb{B}_{22} + \lambda_{\bar{g}}\,\mathbb{B}_{32} \\ \lambda_{\bar{f}}\,\mathbb{B}_{23} + \lambda_{\bar{g}}\,\mathbb{B}_{33} + \lambda_{\bar{h}}\,\mathbb{B}_{43} + \lambda_{\bar{k}}\,\mathbb{B}_{53} + \lambda_{\bar{L}}\,\mathbb{B}_{63} \end{bmatrix} \tag{42}$$

According to the Pontryagin's maximum principle, the optimal control law $\{\tau^\star, \hat{\boldsymbol{\alpha}}^\star\}$, to be selected within the feasible control domain, is designed such that the Hamiltonian $\mathcal{H}$ given by Eq. (38) is an absolute minimum at any time, viz.

$$\hat{\boldsymbol{\alpha}}^\star = -\frac{\boldsymbol{\eta}_{\bar{æ}}}{\|\boldsymbol{\eta}_{\bar{æ}}\|} \tag{43}$$

$$\tau^\star = \frac{1 - \operatorname{sign}(\mathcal{S})}{2} \tag{44}$$

where $\operatorname{sign}(\square)$ is the signum function, and $\mathcal{S}$ is a switching function, defined as

$$\mathcal{S} = -\frac{I_{\rm sp}\,g_0\,\|\boldsymbol{\eta}_{\bar{æ}}\|}{m} - \lambda_m \tag{45}$$

Note that the singular case in which $\mathcal{S} = 0$ (that is, when $\boldsymbol{\lambda}_{\bar{æ}} = \mathbf{0}$), may take place at some isolated points only, and therefore, is not considered in this work. Taking into account Eqs. (41) and (43), the mass costate is $\lambda_m > 0$, which results in $\mathcal{S} < 0$ and $\tau^\star \equiv 1$ during the transfer; see Eq. (44).

The time-optimal trajectory of the deputy is the solution to a two-point boundary-value problem (TPBVP) constituted by 14 first-order differential equations, that is, the equations of motion (32) and (35), and the Euler-Lagrange equations

(40)-(41). The (seven) initial boundary conditions are $\bar{\boldsymbol{\alpha}}_D(t_0) = \bar{\boldsymbol{\alpha}}_0$ and $m_D(t_0) = m_0$, while the (four) final boundary conditions are given by Eqs. (36). The TPBVP is completed by the transversality conditions [41], that is

$$\lambda_m(t_f) = 0, \quad \lambda_{\bar{f}}(t_f)\,\bar{g}_f - \lambda_{\bar{g}}(t_f)\,\bar{f}_f = 0, \quad \lambda_{\bar{L}}(t_f) = 0, \quad \mathcal{H}(t_f) = 0 \tag{46}$$

where t_f is an output of the optimization process. The TPBVP is solved with the procedure proposed by Ref. [40], in which a scaling technique of the initial costate vector (that is, a suitable choice of λ_0) is used to improve the robustness and efficiency of the numerical procedure.

Numerical Simulations

Consider the (slowly rotating) asteroid 4179 Toutatis, whose main physical parameters [29] are reassumed in Table 1. Even though that asteroid actually rotates about a non-principal axis of inertia, it is chosen here as a target object for the numerical simulations to make a meaningful comparison with the literature results [29,30]. The chief spacecraft is assumed to cover a quasi-frozen orbit, of which the feasible region is shown in Fig. 1 as a function of $\{\bar{a}_0, \bar{e}_0\}$. The deputy spacecraft, propelled by a typical cold-gas thruster, is assumed to be a microsatellite with an initial mass $m_0 = 50\,\text{kg}$, a maximum thrust magnitude $T_{\max} = 70\,\text{mN}$, and a specific impulse $I_{\text{sp}} = 60\,\text{s}$.

Table 1 Physical parameters of asteroid 4179 Toutatis [29].

Parameter	Value
μ	$1.79 \times 10^3\ \text{m}^3/\text{s}^2$
n_T	1.34×10^{-5} rad/s
C_{20}	-0.313
C_{22}	0.12
R_0	1.225×10^3 m

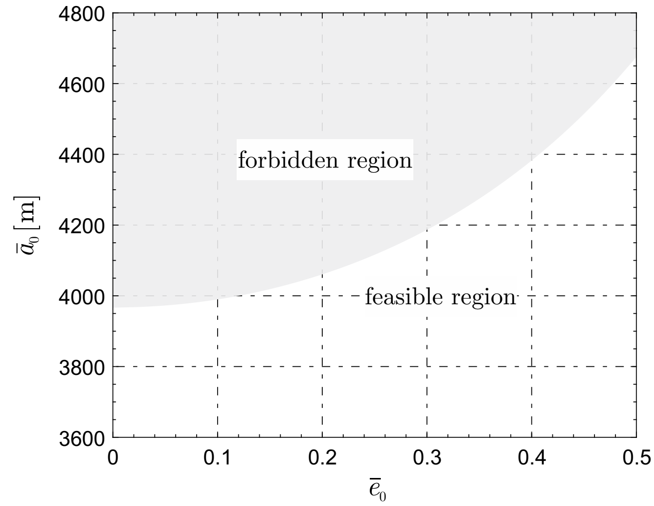

Figure 1 Feasible region for a quasi-frozen orbit around asteroid 4179 Toutatis.

The initial mean orbital elements of the two spacecraft [29] are selected as $\bar{a}_0 = 3.8\,\text{km}$, $\bar{e}_0 = 0.1$, $\bar{i}_0 = 147.48\,\text{deg}$, $\bar{\Omega}_{R_0} = 90\,\text{deg}$, and $\bar{\omega}_0 = \nu_0 = 0\,\text{deg}$. As stated before, the condition $\delta\bar{\Omega}_{R_f} = 0$ must be satisfied to guarantee bounded relative motion. The desired relative eccentricity is chosen equal to $\delta\bar{e}_f = 0.01$, and so the correcting parameter is $\kappa = 1.028$; see Eq. (14). The values of $\delta\bar{a}_f$ and $\delta\bar{i}_f$ are computed from Eqs. (21)–(22) as $\delta\bar{a}_f = -83.1\,\text{m}$ and $\delta\bar{i}_f = -7.2\,\text{deg}$, whereas $\delta\bar{\omega}_f$ and $\delta\nu_f$ are left free.

For convenience, introduce the body-fixed (rotating) reference frame $\mathcal{T}(O; \hat{\boldsymbol{x}}, \hat{\boldsymbol{y}}, \hat{\boldsymbol{z}})$, with origin O coincident with the asteroid center-of-mass, and axes $\{\hat{\boldsymbol{x}}, \hat{\boldsymbol{y}}, \hat{\boldsymbol{z}}\}$ aligned with the minimum, intermediate, and maximum axis of inertia of the asteroid, respectively. The mean orbital elements of the deputy, obtained with a time-optimal control law, are plotted in Fig. 2, while the corresponding components of the thrust unit vector $\hat{\boldsymbol{\alpha}}$ in frame $\mathcal{T}$ are reported in Fig. 3. In this case, a minimum time $t_f = 2.85$ minutes is required to complete the (loose) formation structure with bounded relative motion.

To compare the results with those obtained using the boundedness conditions discussed in Ref. [29], the time history of the relative distance $\rho = \|\boldsymbol{\rho}\|$ between the two spacecraft is illustrated in Fig. 4(a) for a time interval of 30 hours. In addition, Fig. 4(b) shows the minimum time t_f necessary for a loose formation to be constituted as a function of the initial mean eccentricity $\bar{e}_0 \in [0.01,\ 0.1]$. In particular, Fig. 4 clearly shows that the proposed approach guarantees a formation flying with bounded relative distance, and has a better performance in terms of required relative drift and time when compared to the approach proposed in Ref. [29].

Let $\boldsymbol{r} \triangleq [r_x,\ r_y,\ r_z]^{\mathrm{T}}$ denote the position vector of the deputy spacecraft along three coordinate axes in frame $\mathcal{T}$, and let $\boldsymbol{\rho} \triangleq [\rho_x,\ \rho_y,\ \rho_z]^{\mathrm{T}}$ be the relative position vector of the deputy with respect to the chief spacecraft. Figure 5(a) illustrates the time-optimal trajectory necessary to establish bounded relative motion for a maximum thrust value of $T_{\max} = 70\,\text{mN}$, while Fig. 5(b) shows the relative trajectories in the (ρ_y, ρ_z) plane when $T_{\max} = \{10,\ 40,\ 70\}$ mN. The minimum flight time t_f is shown in Fig. 6(a) as a function of $\bar{e}_0 \in [0.01,\ 0.1]$ and $T_{\max} \in [10,\ 100]$ mN, while the corresponding mass variation $\Delta m = \Delta m(\bar{e}_0,\ T_{\max})$ is reported in Fig. 6(b). In particular, Fig. 6 suggests that an

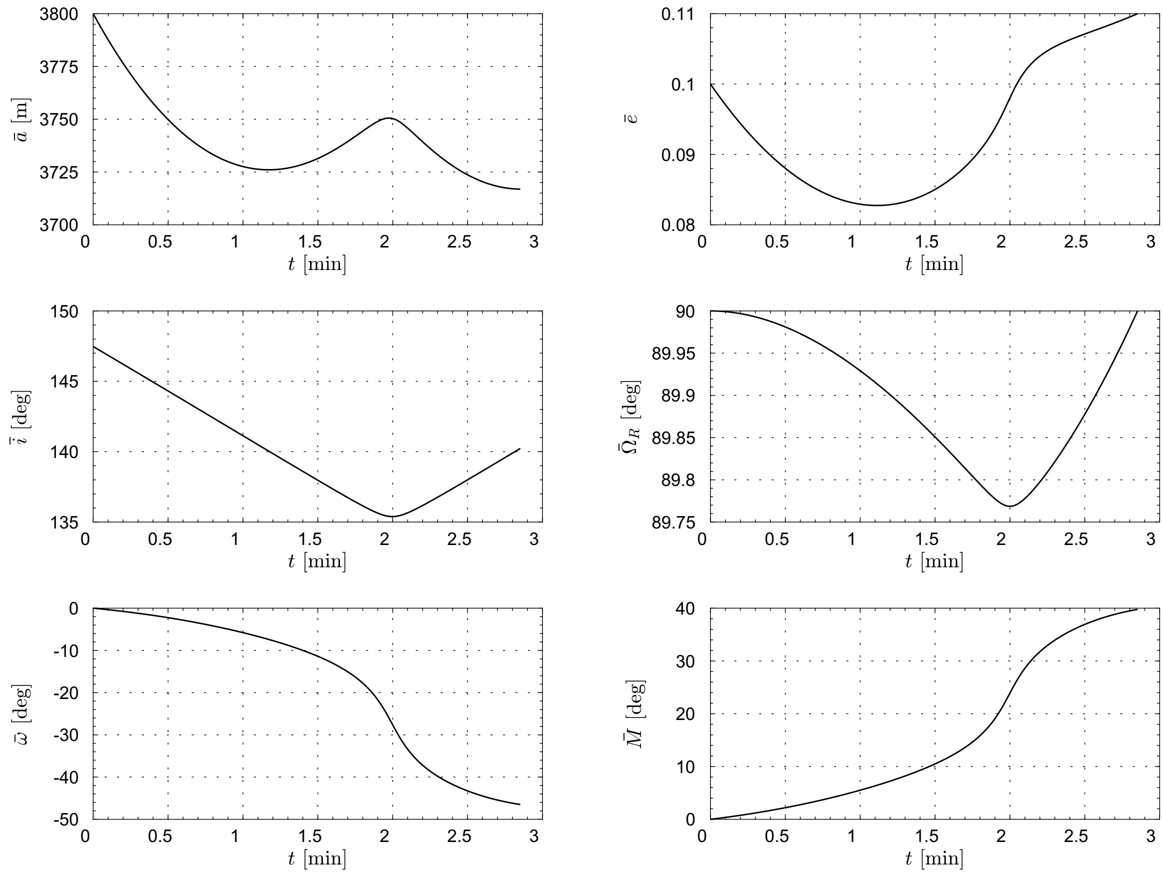

Figure 2 Time histories of mean orbital elements of the deputy spacecraft during the transfer.

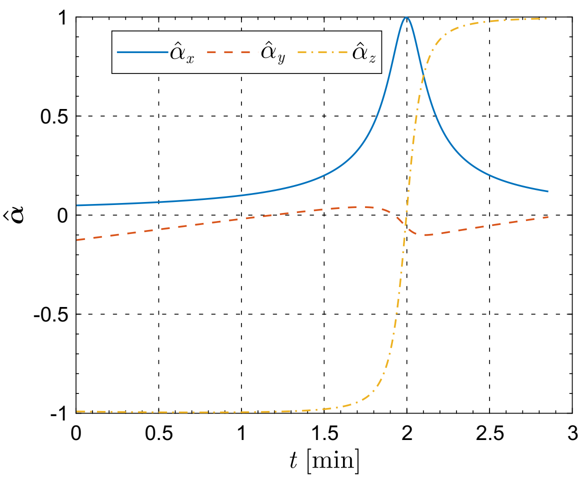

Figure 3 Thrust unit vector components in $\mathcal{T}$ of the deputy spacecraft during the transfer.

initial nominal quasi-frozen orbit with a small eccentricity is preferable, as it requires a shorter flight time and a smaller propellant mass.

Conclusions

Using the mean orbital elements, we have analytically derived the necessary conditions that guarantee bounded spacecraft relative motion around a slowly rotating asteroid, which is schematized as an ellipsoid with uniform density. These conditions are useful for alleviating the mutual drift of the formation flying spacecraft. Based on these constraints, the problem of formation establishment has been addressed within a time-optimal framework by using an indirect approach. The proposed method provides an important reference for the design of a loose formation in the vicinity of a slowly rotating asteroid of regular shape, and represents the starting point for the project of a cluster flight comprised of multiple spacecraft.

It is worth mentioning that the proposed methodology relies on an approximate second-degree and second-order gravitational field, which inevitably gives rise to inherent errors in a real mission scenario. In addition, when dealing with a more accurate irregular gravity field, an analytical approach might be no longer feasible. In that case, numerical

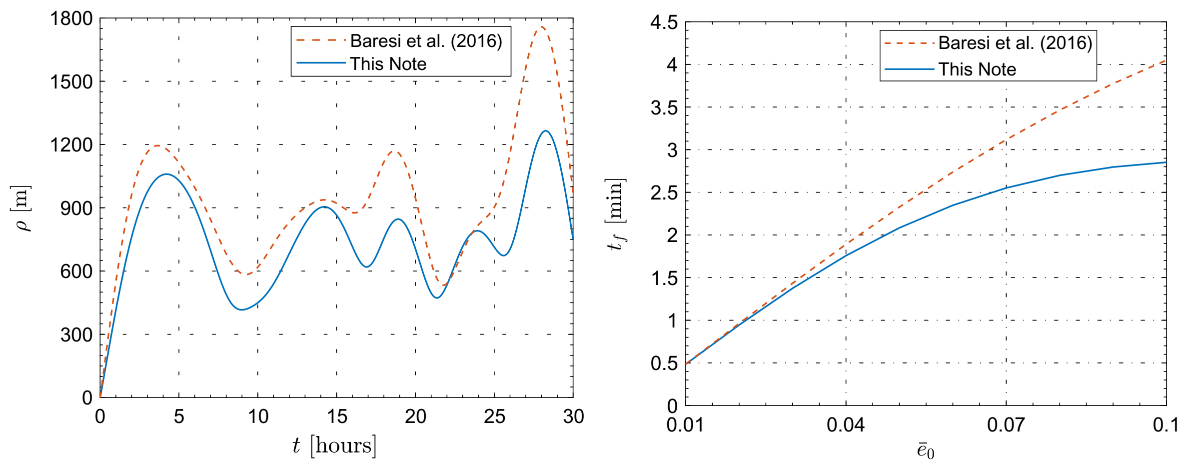

a) Relative distance. **b)** Minimum required time.

Figure 4 Comparison with the literature results [29].

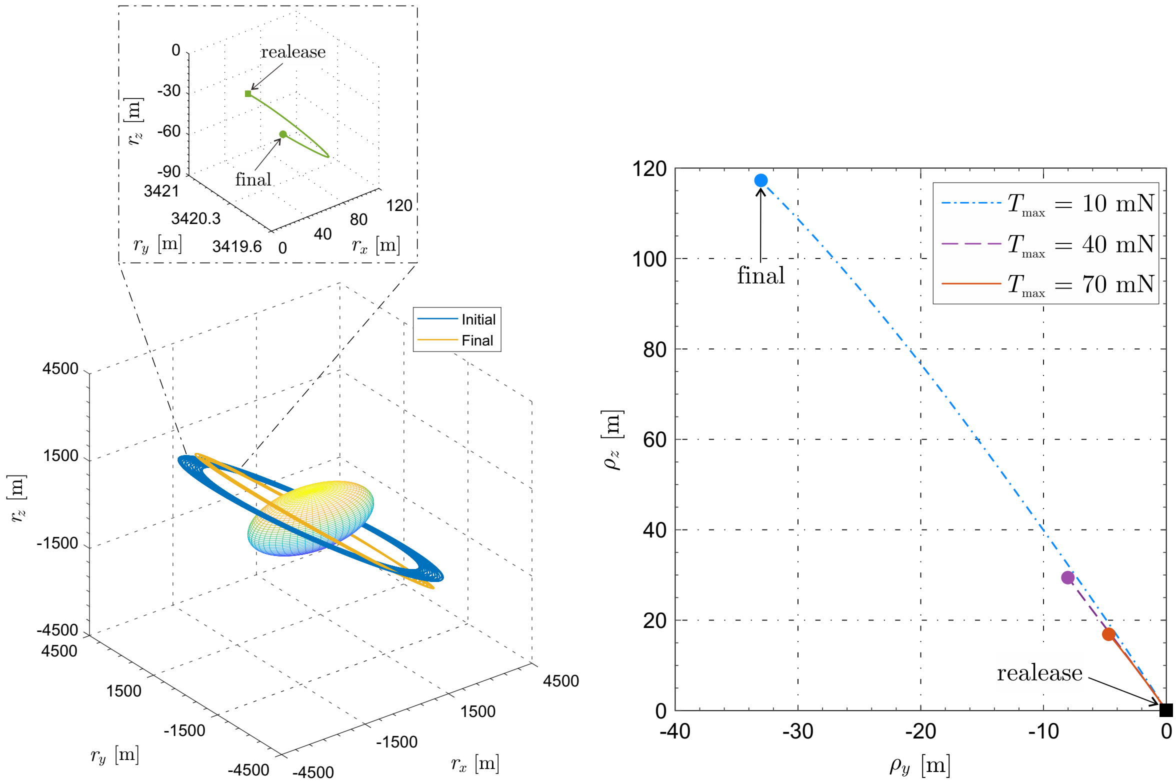

a) Time-optimal trajectory in $\mathcal{T}$. **b)** Projection of relative trajectories in (ρ_y, ρ_z) plane.

Figure 5 Time-optimal trajectories for formation establishment.

(possibly time-consuming) techniques, such as that discussed in the recent literature by Baresi et al., represent an essential tool to analyze the actual spacecraft trajectory.

Acknowledgment

This work was supported by the National Natural Science Foundation of China (Grant nos. 11525208 and 11902175), Postdoctoral Science Foundation of China (Grant nos. BX20190166 and 2019M650700). The authors would like to appreciate the mean-to-osculating orbital elements transformation provided by Hanlun Lei, School of Astronomy and Space Science, Nanjing University.

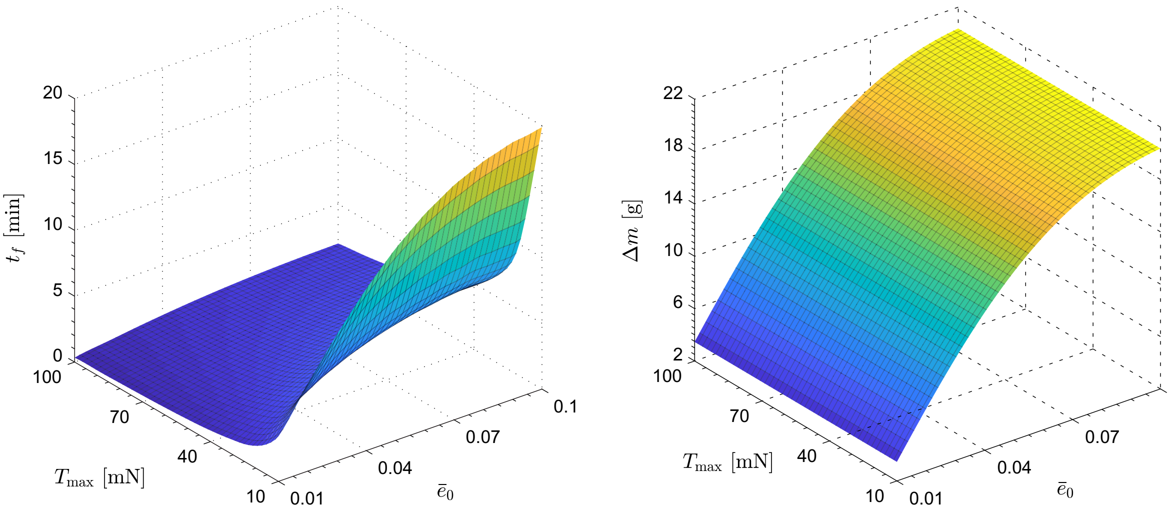

a) Minimum flight time t_f.

b) Propellant mass Δm.

Figure 6 Minimum flight time and corresponding propellant mass required for formation establishment as a function of $(\bar{e}_0, T_{\max})$.

Appendix: Partial Derivatives in Eqs. (8)–(11)

The partial derivatives of $\{\mathcal{F}_{\bar{i}}, \mathcal{F}_{\bar{\Omega}_R}, \mathcal{F}_{\bar{\omega}}, \mathcal{F}_{\bar{M}}\}$ with respect to $\{\bar{a}, \bar{e}, \bar{i}, \bar{\Omega}_R\}$ in Eqs. (8)–(11) are

$$\frac{\partial \mathcal{F}_{\bar{i}}}{\partial \bar{a}} = -\frac{21}{2} C_{22} R_0^2 \mu^{\frac{1}{2}} \bar{a}^{-\frac{9}{2}} \left(1-\bar{e}^2\right)^{-2} \sin\bar{i} \sin 2\bar{\Omega}_R \tag{.1}$$

$$\frac{\partial \mathcal{F}_{\bar{i}}}{\partial \bar{e}} = 12 C_{22} R_0^2 \mu^{\frac{1}{2}} \bar{a}^{-\frac{7}{2}} \left(1-\bar{e}^2\right)^{-3} \bar{e} \sin\bar{i} \sin 2\bar{\Omega}_R \tag{.2}$$

$$\frac{\partial \mathcal{F}_{\bar{i}}}{\partial \bar{i}} = 3 C_{22} R_0^2 \mu^{\frac{1}{2}} \bar{a}^{-\frac{7}{2}} \left(1-\bar{e}^2\right)^{-2} \cos\bar{i} \sin 2\bar{\Omega}_R \tag{.3}$$

$$\frac{\partial \mathcal{F}_{\bar{i}}}{\partial \bar{\Omega}_R} = 6 C_{22} R_0^2 \mu^{\frac{1}{2}} \bar{a}^{-\frac{7}{2}} \left(1-\bar{e}^2\right)^{-2} \sin\bar{i} \cos 2\bar{\Omega}_R \tag{.4}$$

$$\frac{\partial \mathcal{F}_{\bar{\Omega}_R}}{\partial \bar{a}} = -\frac{21}{4} R_0^2 \mu^{\frac{1}{2}} \bar{a}^{-\frac{9}{2}} \left(1-\bar{e}^2\right)^{-2} \cos\bar{i} \left(C_{20} + 2 C_{22} \cos 2\bar{\Omega}_R\right) \tag{.5}$$

$$\frac{\partial \mathcal{F}_{\bar{\Omega}_R}}{\partial \bar{e}} = 6 R_0^2 \mu^{\frac{1}{2}} \bar{a}^{-\frac{7}{2}} \left(1-\bar{e}^2\right)^{-3} \bar{e} \cos\bar{i} \left(C_{20} + 2 C_{22} \cos 2\bar{\Omega}_R\right) \tag{.6}$$

$$\frac{\partial \mathcal{F}_{\bar{\Omega}_R}}{\partial \bar{i}} = -\frac{3}{2} R_0^2 \mu^{\frac{1}{2}} \bar{a}^{-\frac{7}{2}} \left(1-\bar{e}^2\right)^{-2} \sin\bar{i} \left(C_{20} + 2 C_{22} \cos 2\bar{\Omega}_R\right) \tag{.7}$$

$$\frac{\partial \mathcal{F}_{\bar{\Omega}_R}}{\partial \bar{\Omega}_R} = -6 C_{22} R_0^2 \mu^{\frac{1}{2}} \bar{a}^{-\frac{7}{2}} \left(1-\bar{e}^2\right)^{-2} \cos\bar{i} \sin 2\bar{\Omega}_R \tag{.8}$$

$$\frac{\partial \mathcal{F}_{\bar{\omega}}}{\partial \bar{a}} = \frac{21}{16} R_0^2 \mu^{\frac{1}{2}} \bar{a}^{-\frac{9}{2}} \left(1-\bar{e}^2\right)^{-2} \left(3 C_{20} + 5 C_{20} \cos 2\bar{i} - 2 C_{22} \cos 2\bar{\Omega}_R + 10 C_{22} \cos 2\bar{i} \cos 2\bar{\Omega}_R\right) \tag{.9}$$

$$\frac{\partial \mathcal{F}_{\bar{\omega}}}{\partial \bar{e}} = -\frac{3}{2} R_0^2 \mu^{\frac{1}{2}} \bar{a}^{-\frac{7}{2}} \left(1-\bar{e}^2\right)^{-3} \bar{e} \left(3 C_{20} + 5 C_{20} \cos 2\bar{i} - 2 C_{22} \cos 2\bar{\Omega}_R + 10 C_{22} \cos 2\bar{i} \cos 2\bar{\Omega}_R\right) \tag{.10}$$

$$\frac{\partial \mathcal{F}_{\bar{\omega}}}{\partial \bar{i}} = \frac{15}{4} R_0^2 \mu^{\frac{1}{2}} \bar{a}^{-\frac{7}{2}} \left(1-\bar{e}^2\right)^{-2} \sin 2\bar{i} \left(C_{20} + 2 C_{22} \cos 2\bar{\Omega}_R\right) \tag{.11}$$

$$\frac{\partial \mathcal{F}_{\bar{\omega}}}{\partial \bar{\Omega}_R} = -\frac{3}{2} C_{22} R_0^2 \mu^{\frac{1}{2}} \bar{a}^{-\frac{7}{2}} \left(1-\bar{e}^2\right)^{-2} \left(1 - 5 \cos 2\bar{i}\right) \sin 2\bar{\Omega}_R \tag{.12}$$

$$\frac{\partial \mathcal{F}_{\bar{M}}}{\partial \bar{a}} = \frac{21}{16} R_0^2 \mu^{\frac{1}{2}} \bar{a}^{-\frac{9}{2}} \left(1-\bar{e}^2\right)^{-\frac{3}{2}} \left(C_{20} + 3\,C_{20} \cos 2\,\bar{i} - 6\,C_{22} \cos 2\,\bar{\Omega}_R + 6\,C_{22} \cos 2\,\bar{i} \cos 2\,\Omega_R\right) - \frac{3}{2} \mu^{\frac{1}{2}} \bar{a}^{-\frac{5}{2}} \tag{.13}$$

$$\frac{\partial \mathcal{F}_{\bar{M}}}{\partial \bar{e}} = -\frac{9}{8} R_0^2 \mu^{\frac{1}{2}} \bar{a}^{-\frac{7}{2}} \left(1-\bar{e}^2\right)^{-\frac{5}{2}} \bar{e} \left(C_{20} + 3\,C_{20} \cos 2\,\bar{i} - 6\,C_{22} \cos 2\,\bar{\Omega}_R + 6\,C_{22} \cos 2\,\bar{i} \cos 2\,\bar{\Omega}_R\right) \tag{.14}$$

$$\frac{\partial \mathcal{F}_{\bar{M}}}{\partial \bar{i}} = \frac{9}{4} R_0^2 \mu^{\frac{1}{2}} \bar{a}^{-\frac{7}{2}} \left(1-\bar{e}^2\right)^{-\frac{3}{2}} \sin 2\,\bar{i} \left(C_{20} + 2\,C_{22} \cos 2\,\bar{\Omega}_R\right) \tag{.15}$$

$$\frac{\partial \mathcal{F}_{\bar{M}}}{\partial \bar{\Omega}_R} = -\frac{9}{2} C_{22} R_0^2 \mu^{\frac{1}{2}} \bar{a}^{-\frac{7}{2}} \left(1-\bar{e}^2\right)^{-\frac{3}{2}} \left(1-\cos 2\,\bar{i}\right) \sin 2\,\bar{\Omega}_R \tag{.16}$$

References

[1] Farquhar, R., Kawaguchi, J., Russell, C. T., Schwehm, G., Veverka, J., and Yeomans, D., "Spacecraft Exploration of Asteroids: The 2001 Perspective," *Asteroids III*, University of Arizona Press, Tucson, March 2002, pp. 367–376.

[2] Cheng, A. F., Santo, A. G., Heeres, K. J., Landshof, J. A., Farquhar, R. W., Gold, R. E., and Lee, S. C., "Near-Earth Asteroid Rendezvous: Mission Overview," *Journal of Geophysical Research: Planets*, Vol. 102, No. E10, October 1997, pp. 23695–23708. doi: 10.1029/96JE03364.

[3] DeMeo, F. E. and Carry, B., "Solar System Evolution from Compositional Mapping of the Asteroid Belt," *Nature*, Vol. 505, January 2014, pp. 629–634. doi: 10.1038/nature12908.

[4] Scheeres, D. J., *Orbital Motion in Strongly Perturbed Environments: Applications to Asteroid, Comet and Planetary Satellite Orbiters*, chap. 1–2, Springer-Praxis, London, UK, 2012, pp. 3–22, 41–52, ISBN: 978-3-642-03255-4.

[5] Baker, J., "The Falcon Has Landed," *Science*, Vol. 312, No. 5778, June 2006, pp. 1327. doi: 10.1126/science.312.5778.1327.

[6] Arakawa, M., Saiki, T., Wada, K., and et al., "An Artificial Impact on the Asteroid (162173) Ryugu Formed a Crater in the Gravity-Dominated Regime," *Science*, Vol. 368, No. 6486, April 2020, pp. 67–71. doi: 10.1126/science.aaz1701.

[7] Tsuda, Y., Saiki, T., Saiki, T., Nakazawa, S., and Watanabe, S., "Hayabusa2–Sample Return and Kinetic Impact Mission to Near-Earth Asteroid Ryugu," *Acta Astronautica*, Vol. 156, March 2019, pp. 387–393. doi: 10.1016/j.actaastro.2018.01.030.

[8] Truszkowski, W., Hinchey, M., Rash, J., and Rouff, C., "NASA's Swarm Missions: the Challenge of Building Autonomous Software," *IT Professional*, Vol. 6, No. 5, September–October 2004, pp. 301–327. doi: 10.1109/MITP.2004.66.

[9] Gong, S., Li, J., and Baoyin, H., "Formation Flying Solar-Sail Gravity Tractors in Displaced Orbit for Towing Near-Earth Asteroids," *Celestial Mechanics and Dynamical Astronomy*, Vol. 105, No. 1–3, November 2009, pp. 159–177. doi: 10.1007/s10569-009-9211-8.

[10] Vasile, M. and Maddock, C. A., "Design of a Formation of Solar Pumped Lasers for Asteroid Deflection," *Advances in Space Research*, Vol. 50, No. 7, October 2012, pp. 891–905. doi: 10.1016/j.asr.2012.06.001.

[11] Yoo, S., Song, Y., Park, S., and Choi, K., "Spacecraft Formation Flying for Earth-Crossing Object Deflections Using a Power Limited Laser Ablating," *Advances in Space Research*, Vol. 43, No. 12, June 2009, pp. 1873–1889. doi: 10.1016/j.asr.2009.03.025.

[12] Foster, C., Bellerose, J., Mauro, D., and Jaroux, B., "Mission Concepts and Operations for Asteroid Mitigation Involving Multiple Gravity Tractors," *Acta Astronautica*, Vol. 90, No. 1, November 2013, pp. 112–118. doi: 10.1016/j.actaastro.2012.10.010.

[13] Wang, W., Wu, D., Mengali, G., Quarta, A. A., and Baoyin, H., "Asteroid Hovering Missions from a Fuel-Consumption Viewpoint," *Journal of Guidance, Control and Dynamics*, Vol. 43, No. 7, July 2020, pp. 1374–1382. doi: 10.2514/1.G005016.

[14] Baresi, N. and Scheeres, D. J., "Bounded Relative Motion Under Zonal Harmonics Perturbations," *Celestial Mechanics and Dynamical Astronomy*, Vol. 127, No. 4, April 2017, pp. 527–548. doi: 10.1007/s10569-016-9737-5.

[15] Wang, W., Yuan, J., Mengali, G., and Quarta, A. A., "Invariant Manifold and Bounds of Relative Motion Between Heliocentric Displaced Orbits," *Journal of Guidance, Control and Dynamics*, Vol. 39, No. 8, August 2016, pp. 1764–1776. doi: 10.2514/1.G001751.

[16] Ren, W. and Beard, R. W., "Decentralized Scheme for Spacecraft Formation Flying via the Virtual Structure Approach," *Journal of Guidance, Control, and Dynamics*, Vol. 27, No. 1, January–February 2004, pp. 73–82. doi: 10.2514/1.9287.

[17] Izzo, D. and Pettazzi, L., "Autonomous and Distributed Motion Planning for Satellite Swarm," *Journal of Guidance, Control, and Dynamics*, Vol. 30, No. 2, March–April 2007, pp. 449–459. doi: 10.2514/1.22736.

[18] Wang, W., Mengali, G., Quarta, A. A., and Yuan, J., "Multiple Solar Sail Formation Flying Around Heliocentric Displaced Orbit via Consensus," *Acta Astronautica*, Vol. 154, January 2019, pp. 256–267. doi: 10.1016/j.actaastro.2018.03.039.

[19] Ren, W., "Formation Keeping and Attitude Alignment for Multiple Spacecraft Through Local Interactions," *Journal of Guidance, Control, and Dynamics*, Vol. 30, No. 2, March–April 2007, pp. 633–638. doi: 10.2514/1.25629.

[20] Wang, W., Mengali, G., Quarta, A. A., and Yuan, J., "Distributed Adaptive Synchronization for Multiple Spacecraft Formation Flying Around Lagrange Point Orbits," *Aerospace Science and Technology*, Vol. 74, March 2018, pp. 93–103. doi: 10.1016/j.ast.2018.01.007.

[21] Schaub, H. and Alfriend, K. T., "J_2 Invariant Relative Orbits for Spacecraft Formations," *Celestial Mechanics and Dynamical Astronomy*, Vol. 79, No. 2, February 2001, pp. 77–95. doi: 10.1023/A:1011161811472.

[22] Xu, M., Wang, Y., and Xu, S., "On the Existence of J_2 Invariant Relative Orbits from the Dynamical System Point of View," *Celestial Mechanics and Dynamical Astronomy*, Vol. 112, No. 4, April 2012, pp. 427–444. doi: 10.1007/s10569-012-9401-7.

[23] Baresi, N. and Scheeres, D. J., "Design of Bounded Relative Trajectories in the Earth Zonal Problem," *Journal of Guidance, Control, and Dynamics*, Vol. 40, No. 12, December 2017, pp. 3075–3087. doi: 10.2514/1.G002603.

[24] He, Y., Armellin, R., and Xu, M., "Bounded Relative Orbits in the Zonal Problem via High-Order Poincaré Maps," *Journal of Guidance, Control, and Dynamics*, Vol. 42, No. 1, January 2019, pp. 91–108. doi: 10.2514/1.G003612.

[25] Kristiansen, R. and Nicklasson, P. J., "Spacecraft Formation Flying: A Review and New Results on State Feedback Control," *Acta Astronautica*, Vol. 65, No. 11-12, December 2009, pp. 1537–1552. doi: 10.1016/j.actaastro.2009.04.014.

[26] Chung, S.-J., Bandyopadhyay, S., Foust, R., Subramanian, G. P., and Hadaegh, F. Y., "Review of Formation Flying and Constellation Missions Using Nanosatellites," *Journal of Spacecraft and Rockets*, Vol. 53, No. 3, May–June 2016, pp. 567–578. doi: 10.2514/1.A33291.

[27] Wang, X., Jiang, Y., and Gong, S., "Analysis of the Potential Field and Equilibrium Points of Irregular-Shaped Minor Celestial Bodies," *Astrophysics and Space Science*, Vol. 353, No. 1, September 2014, pp. 105–121. doi: 10.1007/s10509-014-2022-8.

[28] Hu, W. and Scheeres, D. J., "Spacecraft Motion About Slowly Rotating Asteroids," *Journal of Guidance, Control, and Dynamics*, Vol. 25, No. 4, July–August 2002, pp. 765–775. doi: 10.2514/2.4944.

[29] Baresi, N., Scheeres, D. J., and Schaub, H., "Bounded Relative Orbits About Asteroids for Formation Flying and Applications," *Acta Astronautica*, Vol. 123, June–July 2016, pp. 364–375. doi: 10.1016/j.actaastro.2015.12.033.

[30] Lei, H., Circi, C., Ortore, E., Condoleo, E., and Xu, B., "Quasi-Frozen Orbits Around a Slowly Rotating Asteroid," *Journal of Guidance, Control, and Dynamics*, Vol. 42, No. 4, April 2019, pp. 794–809. doi: 10.2514/1.G003837.

[31] Battin, R. H., *An Introduction to the Mathematics and Methods of Astrodynamics*, chap. 10, AIAA, Reston, 1999, ISBN: 1-56347-342-9.

[32] Dang, Z., Wang, Z., and Zhang, Y., "Improved Initialization Conditions and Single Impulsive Maneuvers for J_2-Invariant Relative Orbits," *Celestial Mechanics and Dynamical Astronomy*, Vol. 121, No. 3, July 2015, pp. 301–327. doi: 10.1007/s10569-014-9601-4.

[33] Gurfil, P. and Lara, M., "Motion Near Frozen Orbits as a Means for Mitigating Satellite Relative Drift," *Celestial Mechanics and Dynamical Astronomy*, Vol. 116, No. 3, July 2013, pp. 213–227. doi: 10.1007/s10569-013-9486-7.

[34] He, Y. and Xu, M., "Bounded Relative Orbits in the Zonal Gravitational Field for Formation Flying," *Journal of Guidance, Control, and Dynamics*, Vol. 41, No. 7, July 2018, pp. 1629–1641. doi: 10.2514/1.G003107.

[35] Lei, H., Circi, C., and Ortore, E., "Secular Dynamics Around Uniformly Rotating Asteroids," *Monthly Notices of the Royal Astronomical Society*, Vol. 485, No. 2, May 2019, pp. 2731–2743. doi: 10.1093/mnras/stz561.

[36] Circi, C., D'Ambrosio, A., Lei, H., and Ortore, E., "Global Mapping of Asteroids by Frozen Orbits: The Case of 216 Kleopatra," *Acta Astronautica*, Vol. 161, August 2019, pp. 101–107. doi: 10.1016/j.actaastro.2019.05.026.

[37] Walker, M. J. H., Ireland, B., and Owens, J., "A Set Modified Equinoctial Orbit Elements," *Celestial Mechanics*, Vol. 36, No. 4, August 1985, pp. 409–419. doi: 10.1007/BF01227493.

[38] Walker, M. J., "Erratum - A Set of Modified Equinoctial Orbit Elements," *Celestial Mechanics*, Vol. 38, No. 4, April 1986, pp. 391–392. doi: 10.1007/BF01238929.

[39] Schaub, H., Vadali, S. R., and Alfriend, K. T., "Spacecraft Formation Flying Control Using Mean Orbital Elements," *Journal of the Astronautical Sciences*, Vol. 48, No. 1, January–March 2000, pp. 69–87.

[40] Jiang, F., Baoyin, H., and Li, J., "Practical Techniques for Low-Thrust Trajectory Optimization with Homotopic Approach," *Journal of Guidance, Control, and Dynamics*, Vol. 35, No. 1, January–February 2012, pp. 245–257. doi: 10.2514/1.52476.

[41] Bryson, A. E. and Ho, Y. C., *Applied Optimal Control*, Hemisphere Publishing Corporation, New York, NY, 1975, pp. 71–89, ISBN: 0-891-16228-3.